Journal of Materials Chemistry A

Accepted Manuscript

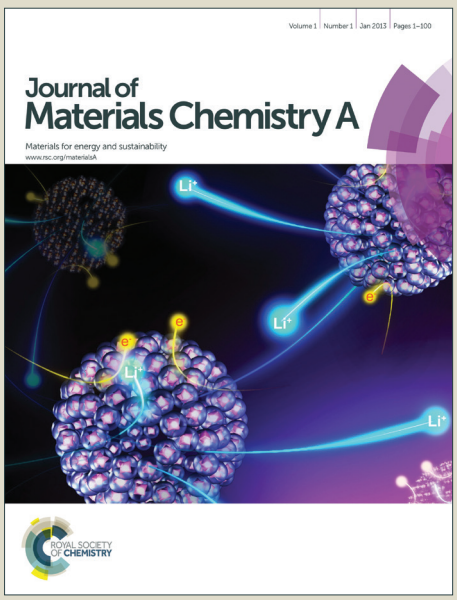

ROYAL SOCIETY OF CHEMISTRY

www.rsc.org/materialsA

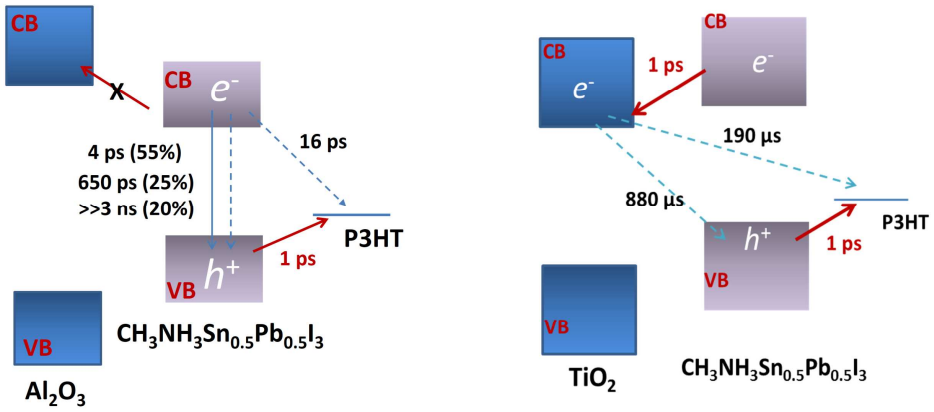

Charge separation and recombination dynamics in Sn/Pb perovskite solar cells were clarified and their relationships to photovoltaic performances were investigated.

Journal of Material Chemistry A RSCPublishing

ARTICLE

Optical Absorption, Charge Separation and Recombination Dynamics in Sn/Pb Cocktail Perovskite Solar Cells and Their Relationships to Photovoltaic Performances

Cite this: DOI: 10.1039/xoxxoooooox

Received ooth January 2012,
Accepted ooth January 2012

DOI: 10.1039/xoxxoooooox

www.rsc.org/

Qing Shen,[*a,e] Yuhei Ogomi,[b,e] Jin Chang,[a,e] Taro Toyoda, [a,e] Kosei Fujiwara,[b] Kenji Yoshino,[c,e] Koki Sato,[a,d] Kouhei Yamazaki,[a] Masaya Akimoto,[a] Yuki Kuga,[a] Kenji Katayama,[d] and Shuzi Hayase[*b,e]

The interest in organometal trihalide perovskite ($CH_3NH_3PbI_3$)-based solid-state hybrid solar cells has increased in recent years due to the high efficiencies achieved, with a record of over 20%, and the simple low temperature preparation method. Further improvements in the photovoltaic performance can be obtained by increasing the light harvesting in the NIR region up to 1000 nm. Recently, successful energy harvesting up to a wavelength of 1060 nm using Sn/Pb cocktail halide based perovskite materials has been achieved. However, the energy conversion efficiency with such solar cells (less than 10%) is much lower than that of $CH_3NH_3PbI_3$ based solar cells, which is due to the lower open circuit voltage (V_{oc}) and fill factor (FF). In order to improve this, we need to have a good understanding of the key factors governing the photovoltaic performance of these solar cells, i.e., the optical absorption, the charge separation and the recombination dynamics. Therefore, for this study, we characterized the optical absorption properties, including the bandgap and the Urbach energy, clarified the photoexcited carrier recombination dynamics in Sn/Pb cocktail perovskite ($CH_3NH_3Sn_{0.5}Pb_{0.5}I_3$) and the charge separation and recombination dynamics at each interface in TiO_2/Sn/Pb perovskite/P3HT solar cells, and lastly investigated the relationships between these and the photovoltaic performance.

Introduction

The interest in organic-inorganic hybrid solid-state solar cells based on organolead halide perovskite has increased over the past three years following the recently reported power conversion efficiency (PCE) of 20.1%.[1-12] Organolead halide perovskites in the form of AMX3 (A=organic molecule, e.g., CH_3NH_3(MA), B=Pb, X=Cl, Br, and I) can be simply crystallized from solution at low temperature (≤100 °C), which enables them to be utilized as light absorbing materials in various solar cells. The higher PCEs of organolead halide perovskites (especially $MAPbI_3$) originate from their unique properties which are critical for high photovoltaic performance: (1) a direct band gap and a high optical absorption coefficient;[13, 14] (2) large dielectric coefficient leading to smaller exciton binding energy (about 20 meV);[15] (3) long photoexcited carrier lifetimes (>100 ns) and long diffusion lengths (100 – 1000 nm even longer);[16, 17] (4) no deep state defects and very small Urbach energy (15 meV).[18] It is expected that further improvements in photovoltaic performance can be obtained by increasing the light harvesting up to NIR wavelengths of 1000 nm, since $MAPbI_3$ perovskite only absorbs light at wavelengths below 800 nm due to its optical band gap of 1.5 eV. Also, from a practical point of view, lead-free organometal halide perovskites are preferable because of the potential toxicology issue of lead. Replacing Pb with Sn or mixing Pb and Sn in organometal halide perovskites can increase the light harvesting in the NIR region up to 1000 nm[19, 20] and reduce the toxicity problem associated with Pb.

Very recently, several groups have studied Sn-based or Pb/Sn cocktail $MASn_xPb_{1-x}I_3$ ($0 \leqq x \leqq 1$) perovskite solar cells.[21-24] The groups of Kanatzidis[21] and Snaith[22] reported $CH_3NH_3SnI_3$ perovskite solar cells with PCEs of about 6%, in which mesoporous TiO_2 was used as a scaffold and spiro-OMeTAD was used as a hole transport material (HTM). However, Sn in its 2+ oxidation state is very sensitive to air, which results in a poor stability of $CH_3NH_3SnI_3$ perovskite solar cells. Hayase et al. was the first to report $MASn_xPb_{1-x}I_3$ ($0 \leqq x \leqq 1$) cocktail perovskite solar cells, in which TiO_2 and P3HT were used as a mesoporous scaffold and a HTM, respectively.[23] They demonstrated energy harvesting in the NIR region using a Sn/Pb cocktail halide perovskite covering wavelengths up to 1060 nm and obtained a maximum efficiency of 4.18 % for $MASn_{0.5}Pb_{0.5}I_3$. They also found the stability of Sn/Pb cocktail halide perovskite solar cells to be better than that of $CH_3NH_3SnI_3$ perovskite solar cells. Kanatzidis et al. also reported $MASn_xPb_{1-x}I_3$ perovskite solar cells, in which spiro-OMeTAD was used as a HTM and a PCE of about 7% obatined.[24] Zou et al. reported planar-heterojunction hybrid $CH_3NH_3Pb_{1-a}Sn_aI_{3-x}Cl_x$ perovskite solar cells, in which PEDOT:PSS and PCBM were used as the HTM and electron transport material (ETM), respectively. A

maximum PCE of 9.7% was achieved for a=0.15 (15% Sn), although the PCE was only 0.04-0.11% for a≥0.5.[25] However, the PCE of Sn/Pb cocktail $MASn_xPb_{1-x}I_3$ perovskite solar cells is much lower than that of $MAPbI_3$ perovskite solar cells. To improve the photovoltaic performance of Sn/Pb cocktail perovskite solar cells, a thorough understanding of the optical absorption properties, the photoexcited carrier lifetimes, and the charge separation and recombination dynamics at each interface is needed.

In this study, we systematically studied the optical absorption, photoexcited carrier lifetime, the charge separation and charge recombination at each interface in Sn/Pb cocktail $MASn_{0.5}Pb_{0.5}I_3$ perovskite solar cells. The relationship of each of these phenomena to the photovoltaic performance of the solar cells was clarified. In the solar cell devices, P3HT was used as the HTM and mesoporous TiO_2 was used as the ETM. We found that the Urbach energy of Sn/Pb cocktail perovskite (34 meV) was more than twice that of $MAPbI_3$ perovskite. Fast recombination (lifetime: 4 ps) of 55% of the photoexcited carriers was observed in the Sn/Pb cocktail perovskite. In addition, charge recombination in the solar cells became faster (the recombination lifetime decreased from 880 μs to 190 μs) when P3HT was used as the HTM. Our results provide detailed relationships between these essential properties and the photovoltaic performance of Sn/Pb cocktail perovskite solar cells and clarify the mechanisms for the poorer PCE, which sheds light on how further improvements in the performance of these solar cells can be made.

Experimental

Sample Preparation.

The Sn/Pb cocktail perovskite samples were fabricated using the following processes and materials.[23] PbI_2 (Purity: 99.999 %), SnI_2, and regioregular poly(3-hexylthiophene-2,5-diyl) (P3HT) were purchased from Sigma Aldrich and used without further purification. F-doped SnO_2 coated glass ((FTO glass), Nippon Sheet Glass Co. Ltd) was patterned using Zn and a 6N HCl aqueous solution. Titanium diisopropoxide bis(acetylacetonate) solution in ethanol was sprayed onto this patterned glass at 300 °C to produce a compact TiO_2 layer. The substrate was dipped in a 40 mM solution of $TiCl_4$ in water for 30 min. followed by baking at 500 °C for 20 min. A porous TiO_2 layer was created by spin-coating with TiO_2 paste (PST-18NR, JGC Catalysts and Chemicals Ltd.) in ethanol (TiO_2 paste: ethanol = 2:7 weight ratio), followed by heating the substrate at 550 °C for 30 min. For some TA measurements, glasses other than FTO, with a porous Al_2O_3 layer deposited on them, were used as substrates. The substrates were spin-coated with a mixture of SnI_2, PbI_2, and CH_3NH_3I (0.5 : 0.5 : 1.0 (mol ratio)) in dimethylformamide (DMF) (40 wt %), followed by baking at 70 °C for 30 min. Then, a solution of P3HT in chlorobenzene (15 mg/ml) was spin coated on the perovskite layer and the substrate was held at room temperature for 1 h in a N_2 atmosphere. For the TA measurements samples of Sn/Pb cocktail perovskite deposited on both Al_2O_3 and TiO_2 with and without P3HT as a HTM were used. Ag and Au electrodes were deposited by vacuum deposition in order to characterize the photovoltaic performance. The photovoltaic performance was evaluated using an AM 1.5G 100 mW/cm^2 irradiance solar simulator (CEP-2000SRR, Bunkoukeiki Inc) with a 0.4 cm x 0.4 cm mask.

Optical Absorption Measurements.

The optical absorption properties of the samples were studied using a gas-microphone photoacoustic (PA) technique.[26] A 300 W xenon arc lamp was used as the light source. A monochromatic light beam was obtained by passing the light through a monochromator. This beam was modulated with a mechanical chopper and focused onto the surface of a sample placed inside a sealed PA cell with nitrogen gas. PA spectrum measurements were carried out within the wavelength range of 500–1200 nm with a modulation frequency of 33 Hz at room temperature. The PA signal was measured by first passing the microphone output through a preamplifier and then to a lock-in amplifier. The PA spectra were normalized using the PA spectrum from a carbon black sheet.

Transient Absorption (TA) Measurements

Two kinds of TA setup were used to characterize the charge separation (electron and hole injection) (a fs TA technique: fs-TA)[27, 28] and the charge recombination dynamics (a ns TA technique: ns-TA)[28-31] in the samples. In the fs-TA setup, the laser source was a titanium/sapphire laser (CPA-2010, Clark-MXR Inc.) with a wavelength of 775 nm, a repetition rate of 1 kHz, and a pulse width of 150 fs. The light was separated into two parts. One part was used as a probe pulse. The other part was used to pump an optical parametric amplifier (OPA) (a TOAPS from Quantronix) to generate light pulses with a wavelength tunable from 290 nm to 3 μm. This was used as the pump light to excite the sample. In this study, the pump light wavelength was 470 nm and the probe beam wavelength was 775 nm. In the ns-TA setup, the pump light source was an OPO (Surelite II – 10FP) output excited by a Nd:YAG nanosecond pulse laser (Panther, Continuum, Electro-Optics Inc.). The pulse width was 5 ns, and the repetition rate was 0.5 Hz. We used pulsed light with a wavelength of 470 nm as the pump light to excite the sample. The probe light came from a fiber coupled CW semiconductor laser. According to the reports of Yoshihara et al. and our earlier studies,[31, 32] a probe wavelengths of 658 nm was used to investigate charge recombination between the electrons in TiO_2 and holes in the perovskite. For all measurements, the pump and probe light were irradiated from the glass side and the TA measurements were carried out in a N_2 atmosphere.

Results and Discussion

Optical Absorption Study: Bandgap and Urbach Energy

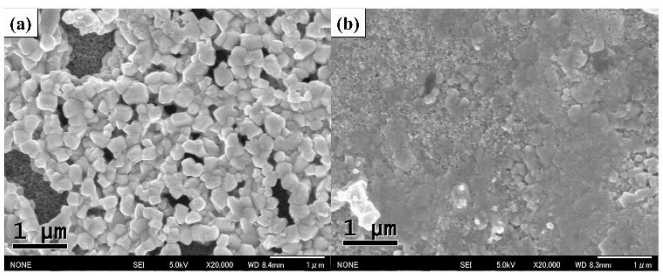

Figure 1. Top-view SEM image of (a) $TiO_2/MASn_{0.5}Pb_{0.5}I_3$ perovskite and (b) $TiO_2/MASn_{0.5}Pb_{0.5}I_3$ perovskite/P3HT samples. The scale bar is 1 μm in both images.

Figure 1a and 1b show the typical scanning electron microscope (SEM) images of $MASn_{0.5}Pb_{0.5}I_3$ perovskite deposited on TiO_2 substrates before and after the deposition of P3HT layer, respectively. The P3HT film acts as the hole transport layer for carriers excited in the perovskite material. Figure 2 shows the optical absorption spectrum of a Sn/Pb

cocktail perovskite sample on a porous TiO_2 substrate measured using the PA technique (in the following, we refer to this as the PA spectrum) at room temperature. From the position of the shoulder in the PA spectrum, the bandgap energy is determined to be 1.21 eV,[33] which is almost the same as that given in our earlier report.[23] We find that below the shoulder, the absorption coefficient follows an exponential trend. The slope of this exponential tail (known as the Urbach tail) corresponds to the absorption tail states, and is usually quantitatively expressed by the Urbach Energy E_U.[18, 34] Investigation of these exponential tails can afford information on the band structure, the disorder, defects, impurities, and electron-phonon interactions in semiconductor materials. Using the experimental relationship between the optical absorption coefficient α in the exponential tail and the photon energy ($h\upsilon$) (eq. (1)), we can calculate the value of E_U of the sample[34, 35]

$$\alpha = \alpha_0 \exp\left(\frac{h\upsilon - h\upsilon_0}{E_u}\right) \quad (1)$$

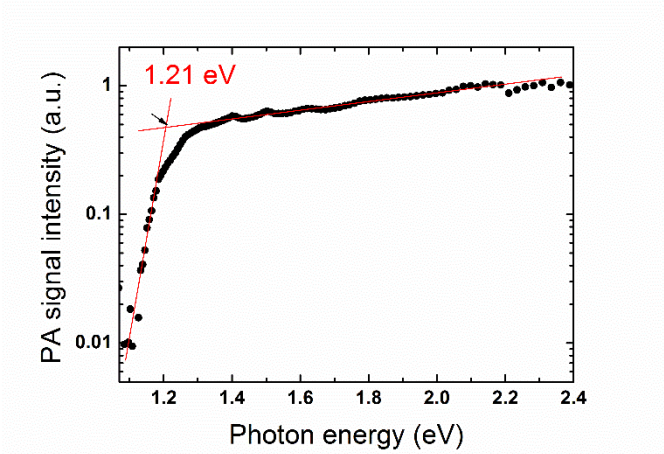

Figure 2. Optical absorption spectrum of Sn/Pb cocktail $MASn_{0.5}Pb_{0.5}I_3$ perovskite measured using a photoacoustic (PA) technique. The bandgap energy and Urbach energy were determined to be 1.21 eV and 34 meV, respectively.

where h is Planck's constant, and α_0, υ_0, E_u are fitting parameters. The value of E_u of Sn/Pb cocktail perovskite was determined to be 34 meV. This is larger than that of Pb perovskite ($CH_3NH_3PbI_3$), which is reported to be 15 meV.[18] We can assume that the value of E_u is a reflection of the disorder and/or defects in the semiconductor crystal.[18, 34-36] Thus, when the density of defects increases, the width of the exponential tail also increases. Therefore, the larger E_u for Sn/Pb cocktail perovskite suggests that there may be higher defect states in the sample compared to $CH_3NH_3PbI_3$. This will result in faster recombination of photoexcited carriers in Sn/Pb cocktail perovskite and lower V_{oc} and *FF*, which we discuss in detail below in conjunction with the TA measurement results.

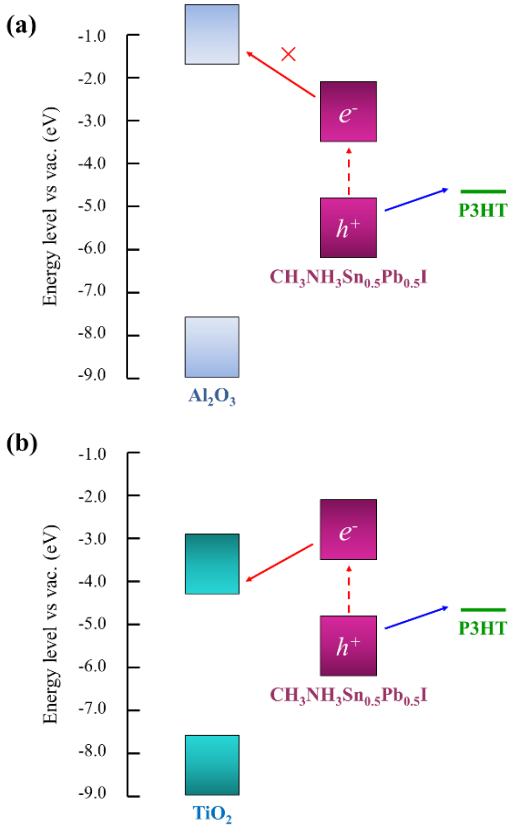

Figure 3. Schematic of relative energy levels in (a) Al_2O_3/Sn/Pb cocktail $MASn_{0.5}Pb_{0.5}I_3$ perovskite/P3HT and (b) TiO_2/Sn/Pb cocktail perovskite $MASn_{0.5}Pb_{0.5}I_3$/P3HT.

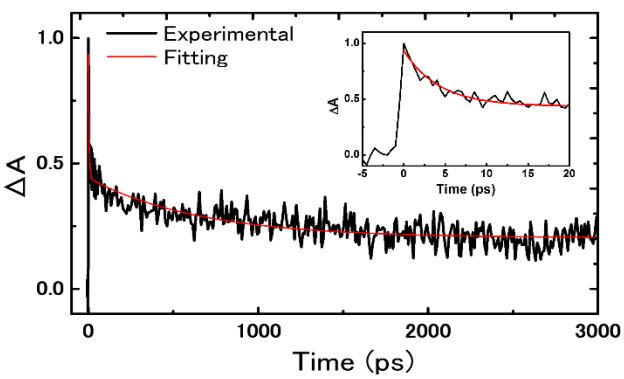

Figure 4. TA response of Sn/Pb cocktail $MASn_{0.5}Pb_{0.5}I_3$ perovskite on Al_2O_3 substrate (black: experimental result; red: fitted result). The inset shows the TA response up to 20 ps.

Dynamics of Photoexcited Carrier Recombination and Hole Transfer to P3HT

To find the mechanism behind the low PCE, especially the low V_{oc} and *FF* in Sn/Pb cocktail perovskite solar cells, which has been reported[23] and is also shown below, we used both the fs-TA and ns-TA techniques to systematically investigate the charge separation and recombination dynamics in these solar cells. TA measurements were conducted on Sn/Pb cocktail perovskite deposited on either Al_2O_3 or TiO_2 films, with and without P3HT. Electrons can be effectively injected from the

perovskite into the conduction band of TiO_2, but this process is impossible in the case of Al_2O_3. This is because the conduction band edge of the perovskite is higher than that of TiO_2 but much lower than that of Al_2O_3 as shown in Figure 3.

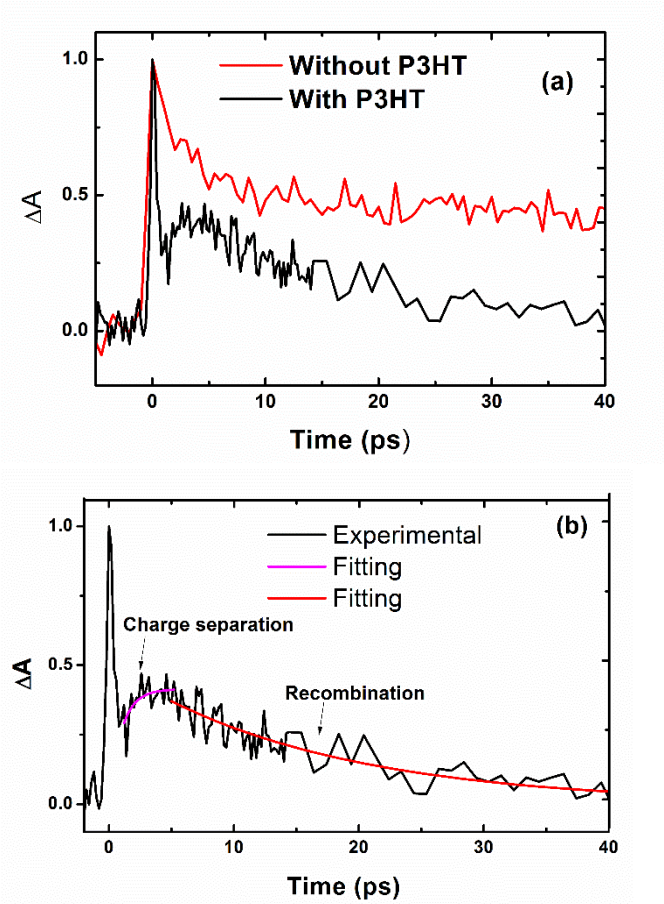

Figure 5. (a) Comparison of normalized TA responses of Sn/Pb cocktail $MASn_{0.5}Pb_{0.5}I_3$ perovskite on an Al_2O_3 substrate without (red) and with (black) P3HT. (b) Experimental and fitted results of the TA response of the sample with P3HT. (Black: experimental; pink: fitted using eq. (3) with a time constant of 1 ps; red: fitted with an exponential function with a time constant of 16 ps.)

For the fs-TA measurements, the pump light wavelength, incident from the glass side, was 470 nm and the probe light wavelength was 775 nm. The TA measurements were carried out under very low pump light intensity (less than 0.5 μJ/cm^2) and all the TA decays were confirmed to be independent of the pump light intensity under such conditions, as reported in detail in our previous paper.[31] In the case of Sn/Pb cocktail perovskite deposited on Al_2O_3, the lifetimes of the photoexcited charge carriers in the perovskite and the charge separation dynamics at the perovskite/P3HT interface were investigated. Figure 4 shows the TA response of the sample over a time scale up to 3 ns. A fast and a slow decay can clearly be observed in the TA response. Because there is no electron injection from the perovskite to the Al_2O_3 owing to the large band gap of Al_2O_3, the decays can be attributed to the recombination processes of photoexcited charge carriers in the perovskite. We found that the TA signal could be well fitted to the following biexponential function:

$$Y = A_1 e^{-t/t_1} + A_2 e^{-t/t_2} + y_0 \qquad (2)$$

where t_1 and t_2 are time constants, A_1 and A_2 are the contributions from the corresponding components, and y_0 is a constant corresponding to a recombination process with a much longer lifetime than the measurement timescale of 3 ns. The time constants t_1 and t_2 of the two charge recombination processes were calculated to be 4.2±0.4 ps ($A_1/(A_1+A_2+y_0)$: 55%) and 650±57 ps ($A_2/(A_1+A_2+y_0)$: 25%), respectively. $y_0/(A_1+A_2+y_0)$ is 20%, which indicates 20% of the photoexcited carriers have a lifetime much longer than 3 ns. These results indicate that the recombination dynamics and lifetimes of photoexcited carriers in Sn/Pb cocktail perovskite are much faster and shorter than those in Pb perovskite (i.e., $CH_3NH_3PbI_3$ and $CH_3NH_3Cl_xI_{3-x}$), which are much greater than 100 ns for more than 90% of the photoexcited carriers.[16, 17, 31] The faster decay processes can be considered to be due to some nonradiative recombination of electrons and holes through defects or trap states in the Pb/Sn cocktail perovskite. This is consistent with the measured larger Urbach energy in Sn/Pb cocktail perovskite (34 meV), which is more than twice as large as that in Pb perovskite (15 mev), as mentioned earlier.

Figure 5 shows the normalized TA responses of the Sn/Pb cocktail perovskite/Al_2O_3 samples with P3HT up to 40 ps, in which a significant difference can be observed compared with that without P3HT. This difference is believed to result from hole injection from the perovskite to the P3HT. For the sample with P3HT, it is very interesting to observe that the TA signal shows a very fast decay accompanied with a fast rise within a few ps, then a peak at around 5 ps followed by a decay with a time constant of about 20 ps. We think the fast rise and fast decay within the first few ps is a result of charge separation at the perovskite/P3HT interface, where the fast rise is due to the generation of $P3HT^+$ due to hole injection from the perovskite to the P3HT layer and the fast decay is due to the decrease of photoexcited carriers in the perovskite. According to other researchers and also our own experimental results,[28, 37] we know that the TA signal probed with 775 nm originates from optical absorption giving rise to the radical P3HT cation ($P3HT^+$), i.e., holes in P3HT. Thus the initial fast rise in the TA signal shown in Fig. 4 (b) reflects the charge separation dynamics, i.e., hole injection into the P3HT layer and the simultaneous generation of $P3HT^+$. The subsequent decrease in the TA signal after 5 ps (after the peak) represents the decrease in the number of holes in the P3HT layer, i.e., the recombination of holes in the P3HT layer with the remaining electrons in the perovskite. The fast rise in the TA signal within 5 ps can be well fitted with the following equation:[28]

$$y = A_1\left(1 - e^{-t/t_1}\right) \qquad (3)$$

where t_1 is the time constant of the rising TA signal, and A_1 is a constant. The time constant t_1 was determined to be 1±0.2 ps, corresponding to the generation time of P3HT. This result means that charge separation at the Sn/Pb cocktail perovskite/P3HT interface occurs within approximately 1 ps. For the TA decay after 5 ps in Fig. 5(b), we find that it can be fitted very well to an exponential function with a decay time of 16 ps. This result indicates that interfacial charge recombination between the Sn/Pb cocktail perovskite (on Al_2O_3 substrate) and P3HT occurs within approximately 16 ps.

Based on the above results, the photoexcited charge carrier dynamics in Sn/Pb cocktail perovskite deposited on Al_2O_3 substrate with and without P3HT as a HTM were clarified. These dynamics are illustrated in Figure 6.

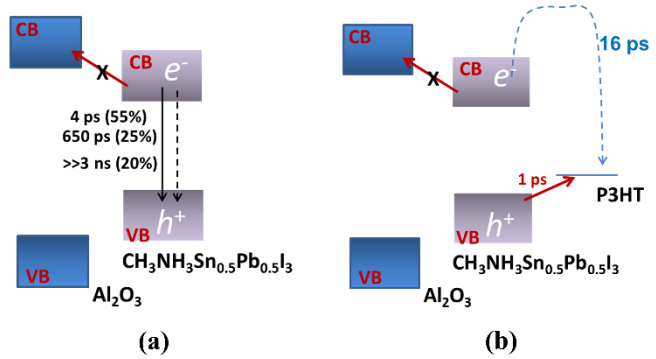

Figure 6. Schematic illustration of photoexcited charge carrier (electrons and holes) dynamics in Sn/Pb cocktail $MASn_{0.5}Pb_{0.5}I_3$ perovskite deposited on an Al_2O_3 substrate without (a) and with (b) P3HT as a hole transport material.

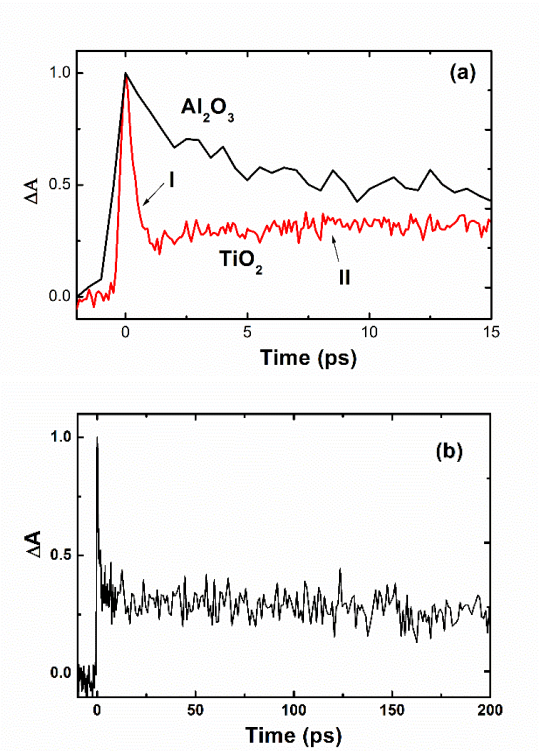

Figure 7. (a) Normalized TA responses of Sn/Pb cocktail perovskite $MASn_{0.5}Pb_{0.5}I_3$ deposited on TiO_2 substrates over time scales of 15 ps (a) and 200 ps (b). For comparison, the TA response of Sn/Pb cocktail perovskite on Al_2O_3 is also shown in (a).

Dynamics of Electron Transfer to TiO_2

Next, we studied the photoexcited electron injection and recombination dynamics of Sn/Pb cocktail perovskite deposited on TiO_2 substrates. Figure 7(a) and (b) shows the normalized TA responses of the sample measured for 15 ps and 200 ps, respectively. For comparison, the TA response of Sn/Pb cocktail perovskite on Al_2O_3 is also shown in Figure 7(a). As shown in Figure 7(a), for Sn/Pb cocktail perovskite on TiO_2, there is a fast decrease in the TA signal (region I) with a time constant of 1 ps (which can be well fitted with an exponential function). This fast decay originates from electron injection from the perovskite to the TiO_2. A simultaneous rise in the TA signal (region II) with a time constant of about 1 ps (which can be well fitted with eq. (3)) can also be clearly observed. This is considered to result from generation of the oxidation state of the Sn/Pb perovskite. Therefore, charge separation at the perovskite/TiO_2 interface occurs in 1 ps. As shown in Figure 7(b), the TA signal is almost unchanged from a few ps to 200 ps, which indicates that no charge recombination occurs at the interface over this timescale. Thus, we measured the charge recombination in Sn/Pb cocktail perovskite deposited on TiO_2 with and without P3HT using the ns-TA setup.

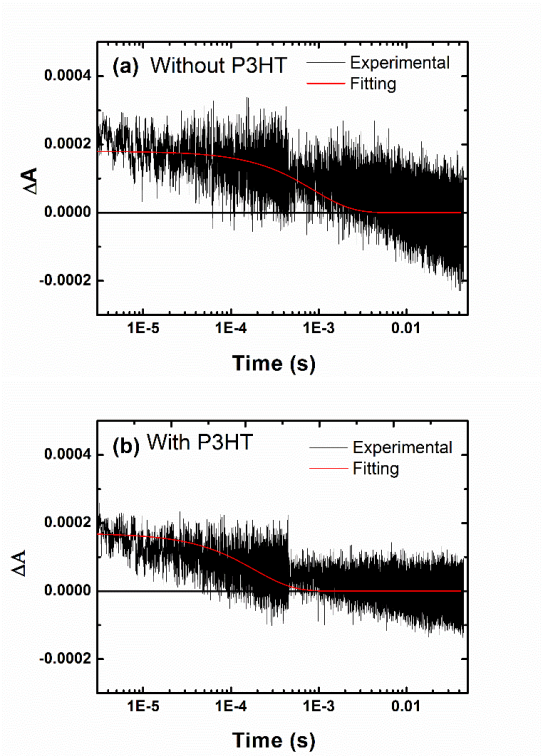

Figure 8. TA responses of Sn/Pb cocktail $MASn_{0.5}Pb_{0.5}I_3$ perovskite deposited on TiO_2 without (a) and with (b) P3HT as a hole transport material measured with a pump light wavelength of 470 nm and a probe light wavelength of 658 nm. The red solid lines shown in (a) and (b) represent exponential decay functions fitted to the results with time constants of 880 μs ((a) without P3HT) and 190 μs ((b) with P3HT), respectively.

Figure 8 shows the TA responses over a time scale of 50 ms of Sn/Pb cocktail perovskite deposited on TiO_2 without (a) and with (b) P3HT as a HTM, which were measured with a pump light wavelength of 470 nm and a probe light wavelength of 658 nm. From previous studies,[29-32] it is known that electrons injected into TiO_2 from sensitizers, such as dyes, quantum dots and perovskite, can be detected by a TA signal probed at 658 nm over timescales from μs to ms. Therefore, it is reasonable to assume that the TA response shown in Figure 8 corresponds to electrons in the TiO_2 injected from the perovskite, since we were unable to observe any TA signal for the samples deposited on Al_2O_3 under the same measurement conditions. So the decay of the TA signal originates from recombination of electrons in the TiO_2 with holes remaining in the Sn/Pb perovskite (Figure 8(a)) or holes in the P3HT (Figure 8(b)). We found the TA response in Figure 8(a) could be well fitted with an exponential function with a time constant of 880 μs. This is a very remarkable result, which means that recombination at the Sn/Pb cocktail perovskite/TiO_2 interface is about two to three orders of magnitude slower compared to that occurring at the

$MAPbI_3/TiO_2$ interface (usually a few μs or less according to our previous studies).[31, 38, 39] As shown in Figure 8(b), the TA response of the sample with P3HT decays much faster compared to that without P3HT, which can be well fitted with an exponential function with a time constant of 190 μs. This result means that recombination of electrons in the TiO_2 is faster when P3HT is used, which originates from recombination at the TiO_2/P3HT interface. This recombination is one of the main reasons for the lower V_{oc} and *FF* of the Sn/Pb cocktail solar cells.[23] Pinhole-free Sn/Pb cocktail perovskite needs to be prepared in order to reduce direct interaction between the TiO_2 and P3HT and thus suppress recombination. The photoexcited charge separation and recombination dynamics of Sn/Pb cocktail perovskite deposited on TiO_2 with P3HT as a HTM were evaluated based on the above results and this is illustrated in Figure 9.

Optical Absorption, Carrier Separation and Recombination Dynamics and their Relationships to the Photovoltaic Performance

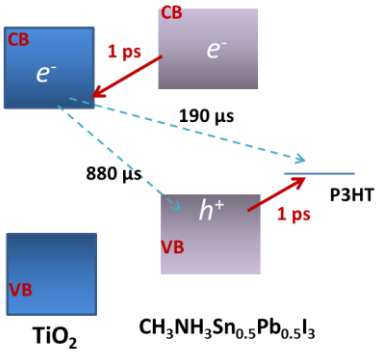

Figure 9. Schematic illustration of photoexcited charge separation and recombination dynamics in Sn/Pb cocktail $MASn_{0.5}Pb_{0.5}I_3$ perovskite solar cells with TiO_2 as an ETM and P3HT as a HTM.

The most important and interesting thing is to understand how the optical absorption, charge separation and recombination dynamics are related to the incident photon to current conversion efficiency (IPCE) spectrum and the current-voltage (I-V) characteristics of the solar cell. Fig. 10(a) shows a typical IPCE spectrum of Sn/Pb cocktail perovskite solar cells. IPCE depends on the optical absorption efficiency η_{Abs}, the charge separation efficiency η_{Csep}, which is the product of the electron injection efficiency η_{Einj} and the hole injection efficiency η_{Hinj}, and the charge collection efficiency η_{Ccol} as follows:

$$IPCE = \eta_{Abs}\eta_{Csep}\eta_{Ccol} = \eta_{Abs}\eta_{Einj}\eta_{Hinj}\eta_{Ccol} \quad (4)$$

Based on the photoexcited carrier relaxation dynamics of Sn/Pb perovskite on Al_2O_3, and the charge transfer dynamics at TiO_2/perovskite/P3HT interfaces (summarized in Table 1), the charge separation efficiency can be calculated. First, the hole injection efficiency η_{Hinj} is almost 100% because the hole injection time constant of 1 ps is many orders of magnitude smaller than the recombination time of 880 μs at the Sn/Pb cocktail perovskite/TiO_2 interface. We can calculate the electron injection efficiency η_{Einj}, as follows. The electron injection time is as fast as 1 ps, therefore all photoexcited electrons with longer lifetimes (650 ps (25%) and >>3 ns (20%)) would be injected into the TiO_2, and only 25% of the photoexcited electrons with the shorter lifetime of 4 ps (55%) would not be injected to TiO_2. Thus, the electron injection efficiency is about 86%. As a result, the charge separation efficiency η_{Csep} (η_{Csep} =$\eta_{Hinj}\eta_{Hinj}$) is 86%. The loss in η_{Csep} (14%) originates from the fast recombination component (lifetime: 4 ps) of photoexcited carriers in the Sn/Pb cocktail perovskite. This may result from nonradiative recombination due to defects in the sample. So the crystalline quality of the Sn/Pb cocktail perovskite needs to be improved in order to achieve 100% charge separation efficiency. The optical absorption is about 95% here, because the perovskite is much more strongly absorbing over a broader range up to 1000 nm, which can enable complete absorption (e.g., at 470 nm) in films as thin as 500 nm.[23] As shown in Fig. 10(a), the IPCE value at 470 nm (the excitation wavelength for the TA measurements in this study) is 68%. Thus, the charge collection efficiency η_{Ccol} is estimated to be 83% from eq. (4). The loss in η_{Ccol} mostly originates from charge recombination occurring at the TiO_2/P3HT interface. To improve *IPCE* and *J*sc, direct contact between the P3HT and the TiO_2 should be suppressed by preparing pinhole-free Sn/Pb cocktail perovskite layers on the TiO_2 or by inserting a barrier at the interface.

Table 1. Photoexcited carrier lifetimes, hole injection and electron injection dynamics as well as charge recombination at each interface in $CH_3NH_3Sn_{0.5}Pb_{0.5}I_3$ perovskite solar cells.

Samples	**Al_2O_3/ $CH_3NH_3Sn_{0.5}Pb_{0.5}I_3$**	**Al_2O_3/ $CH_3NH_3Sn_{0.5}Pb_{0.5}I_3$/ P3HT**	**TiO_2/ $CH_3NH_3Sn_{0.5}Pb_{0.5}I_3$**	**TiO_2/ $CH_3NH_3Sn_{0.5}Pb_{0.5}I_3$/ P3HT**
Charge separation	N/A	Hole injection	Electron injection	Electron/hole injections
		1 ps	1 ps	1 ps/1 ps
Bulk recombination (photoexcited carrier lifetimes)	4 ps (55%) 650 ps (25%) >>3 ns (20%	N/A	N/A	N/A
Interfacial recombination	N/A	16 ps	880 μs	190 μs

As shown in Figure 10(b), J_{sc}, V_{oc}, *FF* and PCE of Sn/Pb cocktail perovskite solar cells are 22.61 mA/cm^2, 0.21 V, 0.37 and 1.77%, respectively. It is clear that the low PCE is mainly because of the low V_{oc} and FF. J_{sc} can be improved to as much as 30 mA/cm^2 if the charge separation efficiency can be increased to 100% by reducing the fast nonradiative recombination rate with a lifetime of 4 ps and if the charge collection efficiency can be increased to more than 95% through suppression of recombination at the TiO_2/P3HT interface. As for V_{oc}, the bandgap-voltage offset $E_G - qV_{oc}$ is as large as 1 eV, where E_G is the bandgap of 1.21 eV, q is the elementary charge. This bandgap-voltage offset is similar to that of amorphous silicon and is considered to be closely related to the larger Urbach energy. The recombination resistance from the I-V curve was estimated to be 27Ω·cm^2, which could also result in lower V_{oc}. The smaller recombination resistance is mostly because of the faster recombination at the TiO_2/P3HT interface. Therefore, we think the lower V_{oc} in Sn/Pb cocktail perovskite solar cells originates from (1) the larger Urbach energy and (2) the smaller recombination resistance. The lower *FF* was also because of the reason (2). Therefore, these findings indicate that the photovoltaic performance of Sn/Pb cocktail perovskite solar cells can be improved by decreasing the Urbach energy, i.e. decreasing the defects in the perovskite, and by reducing the recombination occurring at the TiO_2/P3HT interface through some interface engineering such as passivation or inserting a barrier layer.

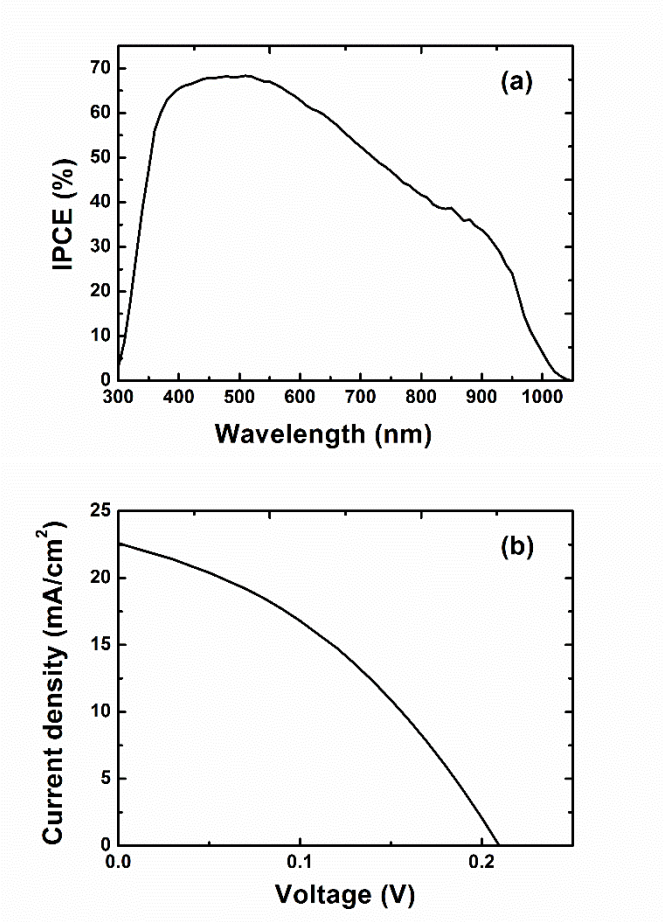

Figure 10. A typical incident photon to current conversion efficiency (IPCE) spectrum (a) and current voltage (I-V) curve (b) of Sn/Pb cocktail $MASn_{0.5}Pb_{0.5}I_3$ perovskite solar cells.

Conclusions

In summary, by undertaking a systematical study of the optical absorption, the photoexcited charge carrier lifetimes, and the charge separation and charge recombination dynamics, we have explored the ways through which the photovoltaic performance of Sn/Pb cocktail $MASn_{0.5}Pb_{0.5}I_3$ perovskite solar cells can be improved. The bandgap was found to be 1.21 eV and light harvesting can be extended to wavelengths over 1000 nm. The Urbach energy was determined to be 34 meV, which is more than twice that of $MAPbI_3$ perovskite. Three recombination processes for the photoexcited carriers were found in the Sn/Pb cocktail perovskite, of which the lifetimes were 4 ps (55%), 650 ps (25%) and one much larger than 3 ns (20%). The larger Urbach energy and the faster recombination indicate there are defects in the Sn/Pb cocktail perovskite. These results are significantly different from those of $MAPbI_3$ perovskite, where the photocarrier lifetimes are larger than 100 ns and almost no defects are observed. On the other hand, the charge separation and charge recombination dynamics were clarified. We found that both electron injection into the TiO_2 and hole transfer to the P3HT layer occurred on timescales of 1 ps. What was surprising was that the charge recombination lifetime at the Sn/Pb cocktail perovskite/TiO_2 interface was as much as 880 µs. This is 2-3 orders of magnitude greater than that occurring at the $MAPbI_3$/TiO_2 interface. However, the charge recombination lifetime was shorter (190 µs) when P3HT was used as a HTM. This suggests that the charge can be more effectively collected without the HTM. Based on the above results, we found that the loss in the charge separation efficiency originates from fast photoexcited carrier recombination with a lifetime of 4 ps, and the loss in charge collection was because of charge recombination occurring at the TiO_2/P3HT interface, leading to lower IPCE values. In addition, the low V_{oc} and *FF* were found to result from the large Urbach energy and recombination occurring at the TiO_2/P3HT interface. These findings indicate that the photovoltaic performance of Sn/Pb cocktail perovskite solar cells can be improved by reducing the defects in the material and the recombination occurring at the TiO_2/HTM interface through some interfacial engineering.

Acknowledgements

This research was supported by the CREST program of Japan Science and Technology Agency (JST).

Notes and references

[a] Department of Engineering Science, Faculty of Informatics and Engineering, The University of Electro-Communications, 1-5-1 Chofugaoka, Chofu, Tokyo 182-8585, Japan. E-mail: shen@pc.uec.ac.jp. Tel: +81 42 443 5471. Fax: +81 42 443 5501.

[b] Graduate School of Life Science and Systems Engineering, Kyushu Institute of Technology, 2-4 Hibikino, Wakamatsu, Kitakyushu 808-0196, Japan. E-mail: hayase@life.kyutech.ac.jp. Tel: +81 93 695 6044, Fax: +81 93 695 6005.

[c] Department of Electrical and Electronic Engineering, Miyazaki University, 1-1 Gakuen, Kibanadai-nishi, Miyazaki 889-2192, Japan.

d Department of Applied Chemistry, Faculty of Science and Engineering, Chuo University, 1-13-27 Kasuga, Bunkyo, Tokyo 112-8551, Japan.

e CREST, Japan Science and Technology Agency (JST), 4-1-8 Honcho, Kawaguchi, Saitama 332-0012, Japan.

1 http://www.nrel.gov/ncpv/.
2 H. S. Jung and N.-G. Park, *Small*, 2014, **11**, 10-25.
3 N. J. Jeon, J. H. Noh, Y. C. Kim, W. S. Yang, S. Ryu and S. I. Seok, *Nat. Mater.*, 2014, **13**, 897-903.
4 H. Zhou, Q. Chen, G. Li, S. Luo, T.-b. Song, H.-S. Duan, Z. Hong, J. You, Y. Liu and Y. Yang, *Science*, 2014, **345**, 542-546.
5 M. A. Green, A. Ho-Baillie and H. J. Snaith, *Nat. Photon*, 2014, **8**, 506-514.
6 M. Z. Liu, M. B. Johnston and H. J. Snaith, *Nature*, 2013, **501**, 395-398.
7 G. E. Eperon, V. M. Burlakov, A. Goriely and H. J. Snaith, *ACS Nano*, 2014, **8**, 591-598.
8 J. Burschka, N. Pellet, S. J. Moon, R. Humphry-Baker, P. Gao, M. K. Nazeeruddin and M. Gratzel, *Nature*, 2013, **499**, 316-319.
9 H. S. Kim, C. R. Lee, J. H. Im, K. B. Lee, T. Moehl, A. Marchioro, S. J. Moon, R. Humphry-Baker, J. H. Yum, J. E. Moser, M. Gratzel and N. G. Park, *Sci. Rep.*, 2012, **2**, 591.
10 M. M. Lee, J. Teuscher, T. Miyasaka, T. N. Murakami and H. J. Snaith, *Science*, 2012, **338**, 643-647.
11 J. H. Im, J. Chung, S. J. Kim and N. G. Park, *Nanoscale Res. Lett.*, 2012, **7**, 353.
12 N. G. Park, *J. Phys. Chem. Lett.*, 2013, **4**, 2423-2429.
13 G. Hodes, *Science*, 2013, **342**, 317-318.
14 H. J. Snaith, *J. Phys. Chem. Lett.*, 2013, **4**, 3623-3630.
15 S. Sun, T. Salim, N. Mathews, M. Duchamp, C. Boothroyd, G. Xing, T. C. Sum and Y. M. Lam, *Energy Environ. Sci.*, 2014, **7**, 399-407.
16 S. D. Stranks, G. E. Eperon, G. Grancini, C. Menelaou, M. J. P. Alcocer, T. Leijtens, L. M. Herz, A. Petrozza and H. J. Snaith, *Science*, 2013, **342**, 341-344.
17 G. C. Xing, N. Mathews, S. Y. Sun, S. S. Lim, Y. M. Lam, M. Gratzel, S. Mhaisalkar and T. C. Sum, *Science*, 2013, **342**, 344-347.
18 S. De Wolf, J. Holovsky, S.-J. Moon, P. Löper, B. Niesen, M. Ledinsky, F.-J. Haug, J.-H. Yum and C. Ballif, *J. Phys. Chem. Lett.*, 2014, **5**, 1035-1039.
19 C. C. Stoumpos, C. D. Malliakas and M. G. Kanatzidis, *Inorg. Chem.*, 2013, **52**, 9019-9038.
20 Y. Takahashi, R. Obara, Z.-Z. Lin, Y. Takahashi, T. Naito, T. Inabe, S. Ishibashi and K. Terakura, *Dalton Trans.*, 2011, **40**, 5563-5568.
21 F. Hao, C. C. Stoumpos, D. H. Cao, R. P. H. Chang and M. G. Kanatzidis, *Nat. Photon*, 2014, **8**, 489-494.
22 N. K. Noel, S. D. Stranks, A. Abate, C. Wehrenfennig, S. Guarnera, A. Haghighirad, A. Sadhanala, G. E. Eperon, S. K. Pathak, M. B. Johnston, a. petrozza, L. Herz and H. Snaith, *Energy Environ. Sci.*, 2014, **7**, 3061-3068.
23 Y. Ogomi, A. Morita, S. Tsukamoto, T. Saitho, N. Fujikawa, Q. Shen, T. Toyoda, K. Yoshino, S. S. Pandey, T. Ma and S. Hayase, *J. Phys. Chem. Lett.*, 2014, **5**, 1004-1011.
24 F. Hao, C. C. Stoumpos, R. P. H. Chang and M. G. Kanatzidis, *J. Am. Chem. Soc.*, 2014, **136**, 8094-8099.
25 F. Zuo, S. T. Williams, P.-W. Liang, C.-C. Chueh, C.-Y. Liao and A. K. Y. Jen, *Adv. Mater.*, 2014, **26**, 6454-6460.
26 A. Rosencwaig and A. Gersho, *J. Appl. Phys.*, 1976, **47**, 64-69.
27 Q. Shen, Y. Ogomi, B.-w. Park, T. Inoue, S. S. Pandey, A. Miyamoto, S. Fujita, K. Katayama, T. Toyoda and S. Hayase, *Phys. Chem. Chem. Phys.*, 2012, **14**, 4605-4613.
28 Q. Shen, Y. Ogomi, S. K. Das, S. S. Pandey, K. Yoshino, K. Katayama, H. Momose, T. Toyoda and S. Hayase, *Phys. Chem. Chem. Phys.*, 2013, **15**, 14370-14376.
29 N. Maeda, H. Hata, N. Osada, Q. Shen, T. Toyoda, S. Kuwahara and K. Katayama, *Phys. Chem. Chem. Phys.*, 2013, **15**, 11006-11013.
30 N. Osada, T. Oshima, S. Kuwahara, T. Toyoda, Q. Shen and K. Katayama, *Phys. Chem. Chem. Phys.*, 2014, **16**, 5774-5778.
31 Q. Shen, Y. Ogomi, J. Chang, S. Tsukamoto, K. Kukihara, O. Takuya, N. Osada, K. Yoshino, K. Katayama, T. Toyoda and S. Hayase, *Phys. Chem. Chem. Phys.*, 2014, **16**, 19984-19992.
32 T. Yoshihara, R. Katoh, A. Furube, Y. Tamaki, M. Murai, K. Hara, S. Murata, H. Arakawa and M. Tachiya, *J. Phys. Chem. B*, 2004, **108**, 3817-3823.
33 J. J. Prías-Barragán, L. Tirado-Mejía, H. Ariza-Calderón, L. Baños, J. J. Perez-Bueno and M. E. Rodríguez, *J. Cryst. Growth*, 2006, **286**, 279-283.
34 F. Urbach, *Phys. Rev.*, 1953, **92**, 1324.
35 K. T. H., *Phys. Rev.*, 1966, **144**, 582.
36 K. S. and N. W., *Phys. Rev. B*, 1999, **59**, 12940.
37 J. Guo, H. Ohkita, H. Benten and S. Ito, *J. Am. Chem. Soc.*, 2010, **132**, 6154-6164.
38 Y. Ogomi, A. Morita, S. Tsukamoto, T. Saitho, Q. Shen, T. Toyoda, K. Yoshino, S. S. Pandey, T. Ma and S. Hayase, *J. Phys. Chem. C*, 2014, **118**, 16651-16659.
39 Y. Ogomi, K. Kukihara, S. Qing, T. Toyoda, K. Yoshino, S. Pandey, H. Momose and S. Hayase, *ChemPhysChem*, 2014, **15**, 1062-1069.

